Beyond-mean-field effects on nuclear triaxiality

Tu Ya,[1,*] Yong-Shou Chen,[2,†] Zao-Chun Gao,[2,3] Ling Liu,[1] and Yong-Jing Chen[2]
[1]*School of Physics science and Technology, Shenyang Normal University, ShenYang 110034, China*
[2]*China Institute of Atomic Energy, Beijing 102413, China*
[3]*State Key Laboratory of Theoretical Physics, Institute of Theoretical Physics, Chinese Academy of Sciences, Beijing 100190, China*
(Received 8 March 2017; published 19 June 2017)

The beyond-mean-field effects on nuclear triaxiality are studied by applying the projected total energy surface (PTES) calculations to the light tungsten isotopes $^{170–178}$W, which have been well described as prolate rotors within the mean-field approximation. The present PTES calculations have well reproduced the experimental energies of the yrast states and the available experimental transition quardrupole moment (Q_t) in function of spin. In particular, the results present a considerable large triaxiality for their ground states, with an average triaxial deformation $\gamma \sim 15^\circ$. For a comparison, the total Routhian surface calculations have also been performed for these nuclei, the results show a well-established axial quadrupole deformation in their ground states. The presence of the significant triaxial deformation can be attributed to the beyond-mean-field effect as the angular momentum projection. This effect is therefore essential for a variety of mean-field approaches since it is only associated with the necessary restoration of the rotational symmetry in the laboratory frame, which is spontaneously broken in the intrinsic frame.

DOI: 10.1103/PhysRevC.95.064316

I. INTRODUCTION

Nuclei are microscopic finite quantum many-body systems that can present collective properties corresponding to specific shapes of the mean field, which can be described by a geometric nuclear surface. The collectivity associated with a quadruple-shaped deformation has been understood as one of the most basic aspects of nuclear structure [1,2]. Mean-field approaches, with the intrinsic spontaneous symmetry breaking mechanism, are widely used to understand the microscopy of the nuclear quadruple deformation. The study of the origin of nuclear equilibrium deformation and its evolution as function of proton and neutron numbers as well as function of spin has long been a subject to attract great theoretical and experimental interest; for a review, see, for example, Ref. [3] and references therein.

The theoretical studies based on the mean-field approximation have been very successful and extracted the conclusion that most of the deformed nuclei show a quadruple deformation of the prolate kind that preserves to a great extent axial symmetry. However, the present study challenges the validity of this conclusion by showing that the significant triaxiality, the axial symmetry breaking, can occur in those nuclei who are predicted by mean-field models to be axial rotors due to the beyond-mean-field effects associated with the angular momentum projection. The mean-field framework can be considered as a useful starting point for microscopic studies of nuclear structure. Mean-field approximations are based on product trial wave functions, which break usually several symmetries of the underlying nuclear Hamiltonian. The full quantum mechanical description of a nuclear state requires the necessary restoration of all these symmetries in the laboratory frame in order to obtain the good quantum numbers for the wave function of the quantum state. The typical example is the restoration of the rotational symmetry, which is broken in the quadruplely deformed mean field, representing the prolate shape, with only one symmetric axis, or the triaxial shape, with no symmetric axis. The rotational symmetry restoration can be realized through angular momentum projection onto the wave function, and this is crucial in description of the quadruple collectivity, such as nuclear high spin states. We will discuss the point in detail below.

To incorporate the beyond-mean-field effects associated with the rotational symmetry restoration, the projected total energy surface (PTES) approach has been recently developed [4] based on the triaxial projected shell model (TPSM) [5], hybridized with the macroscopic-microscopic method. The total energy of an atomic nucleus can be decomposed into the macroscopic, microscopic, and rotational terms. In this model, the macroscopic and microscopic parts are described with the liquid drop model and Strutinsky method of shell effects, respectively, and the rotational energy is given by the TPSM, as the beyond-mean-field term. One well-known approach for the description of the nuclear shape and its evolution in highly rotating nuclei has been the total Routhian surface (TRS) method based on the cranked shell model (CSM). The basic framework of the PTES is similar to the TRS, but the key difference between the two approaches is the fact that the PTES has the energy surface carrying good angular momentum and the TRS provides the energy surface having a semiclassical rotating frequency, not quantum number. In other words, the TRS is a pure mean-field approach while the PTES contains the beyond-mean-field effects associated with the rotational symmetry restoration. The somewhat details about the advantages and disadvantages of two approaches will be discussed in sections below. The major advantage of the PTES approach is manifested by the fact that the energy surfaces correspond to each of given spins so that the

*tuya_sy@126.com
†yschen@ciae.ac.cn

determined nuclear states have a good quantum number of angular momentum and theoretical results, therefore, can be compared directly with the experimental data in the laboratory frame.

The present PTES calculations will focuss on the light tungsten isotopes, $^{170-178}$W even-even nuclei, which have been predicted based on the mean-field approximation, for example, from the TRS calculations, to have an axial quadruple deformation in their ground states. The performed calculation was based on the strategy of adopting axial symmetric shaped system having been well described by the mean-field models as the starting point to investigate the development of the triaxial shapes driven by the beyond mean-field effects associated the necessary rotational symmetry restoration in the laboratory frame. To the date much data have been collected, especially the spectroscopy of the low-lying states in even-even systems with mass number $A = 170$–200. This mass region is particularly interesting because it lies between the doubly magic numbers. These nuclei showing oblate deformation or deformed mass distributions breaking axial symmetry (referred to as triaxial deformation) are of great interest to deepen into the understanding of the shell structure underlying the appearance of deformation. For example, the neutron rich isotopes of Er, Yb, Hf, W, Os, Pt showing a prolate to oblate shape transition as well as best examples of triaxial ground states. These neutron-rich isotopes are, therefore, best quantum many-body systems for the studies of the shape phase transitions, including deformation changes to the oblate and triaxial shapes, whose magnitude depends on the valence nucleons and have been shown to exhibit remarkable fingerprints in spectroscopic observables, for example, see Refs. [6–9]. This transitional region is also characterized by the strong competition between oblate and prolate configurations, i.e., shape coexistence, and of particular interest has been the case of ^{190}W, for example, see Refs. [10–12]. Although the interesting physics in this mass region is rich as mentioned above and those phenomena have been successfully studied based on the mean-field approximation, the beyond-mean-field effects on the nuclear triaxiality have not been studied. we have aimed in the present investigation the impact of the beyond-mean-field effects on the nuclear triaxiality, and for this purpose the light tungsten system is one of best targets for the study because of their characteristics of the prolate rotor predicted in the previous mean-field studies.

In Sec. II, we provide a brief description of the projected total energy surface theory, which incorporates the beyond-mean-field effects in the energy surface calculation. Section III presents the calculated results and the discussions, including the TRS calculation for a comparison. Finally, a summary and conclusion are given in Sec. IV.

II. BRIEF DESCRIPTION OF THE PROJECTED TOTAL ENERGY SURFACE THEORY

The projected total energy surface approach has been developed based on the triaxial projected shell model and hybridized with the macroscopic-microscopic method, in which the total energy of the nuclear system includes three terms,

$$E^{\rm tot} = E_{LD} + E_{\rm corr} + E_{\rm rot}, \tag{1}$$

where E_{LD} is the liquid-drop model energy [13], $E_{\rm corr}$ presents the quantal effects, which is given by the Strutinsky method as the shell correction term [14,15], and sometimes includes the pairing correction. For simplicity and more clear structure of the theory the pairing correction is not considered in the present calculation, and it was checked that inclusion of pairing correction does not change the results of minima although the energy surface becomes a bit complex in the region apart from the minimum. The term of $E_{\rm rot}$ is the rotational energy obtained by the TPSM, which can be further decomposed into the collective rotational term and the quasiparticle (QP) excitation induced by rotation [4]. The basic construction of the total energy is similar to that of the total Routhian in the total Routhian surface (TRS) method where the rotational energy is calculated microscopically as a function of the rotational frequency, namely, the difference between the expectation values of the Hamiltonian at the rotational frequency nonzero and zero by using the cranking wave function, $\langle\Psi^{\omega}|H|\Psi^{\omega}\rangle - \langle\Psi^{\omega=0}|H|\Psi^{\omega=0}\rangle$, see, for example, Refs. [16–19]. In addition, the QP excitation energy is calculated as the sum energy of the excited QPs in the rotating frame at the frequency ω, which belong to the given configuration. A similar construction of the total energy in laboratory frame has been successfully applied to the energy curve calculation, energy in function of elongation deformation, in the studies of the collectivity of neutron rich nuclei [20] and the shape-coexisting rotation of neutron-deficient nuclei [21].

All the terms of Eq. (1), of course, depend on the neutron and proton numbers (N, Z), and the deformation parameters, ε_2, γ, and ε_4, which are not written explicitly. The PTES described with Eq. (1) carries then the good quantum number of angular momentum through the rotational term, and the minimization procedure has to be performed for each given spin. Therefore, the PTES approach may be classified as the variation after projection.

The Hamiltonian of the TPSM is expressed as follows:

$$H = H_0 - \frac{1}{2}\sum_{\lambda=2}^{4}\chi_\lambda \sum_{\mu=-\lambda}^{\lambda} Q^{\dagger}_{\lambda\mu}Q_{\lambda\mu} - G_0 P^{\dagger}_{00}P_{00} - G_2\sum_{\mu=-2}^{2} P^{\dagger}_{2\mu}P_{2\mu}. \tag{2}$$

Where H_0 is the spherical single-particle Hamiltonian, which contains a proper spin orbit force [22]. The second term is the quadrupole-quadrupole (QQ) interaction that includes the *nn*, *pp*, and *np* components. In normal spectroscopic calculation of TPSM, the interaction strength is determined in a self-consistent way with the quadrupole deformation; refer to Ref. [5]. In the energy surface calculation, however, the QQ interaction strength χ should be fixed during the calculation, namely, keeping a constant for each of deformation mesh points. The problem for the adoption of the interaction strength arises then due to hundreds of deformation points. However, unfortunately, the strength value has not yet been given in a

commonly known way. We suggest a rule that this quadrupole interaction strength may be obtained in the self-consistent way of the TPSM theory with respect to a proper one of the deformation mesh points. In the present calculation, the values of the strength χ are determined in the self-consistent way with the equilibrium deformation corresponding to the local minimum of the Strutinsky's energy surface of $E_{LD} + E_{\rm shell}$. Consequently, our PTES calculation has to include two steps, namely, first the Strutinsky's energy surface to obtain the interaction strength and finally the PTES. Note that two kinds of energy surface are not required to have exactly the same mesh structure, and this allows us to reduce the computation time. The third term in the Hamiltonian is the monopole pairing, whose strength parameter G_0 (in MeV) is determined by the expression $G_0 = (g_1 \mp g_2 \frac{N-Z}{A})A^{-1}$, where $g_1 = 20.12$ and $g_2 = 13.13$ was taken in the present calculation, which are suitable for the rare-earth mass region [23], and the minus (plus) sign stands for neutrons (protons). The last term is the quadrupole pairing, whose strength parameter G_2 may be calculated from $G_2 = fG_0$, usually $f = 0$–0.2, we set $f = 0.16$ as an usual value. In the present calculation, the hexadecapole deformation is not considered as a variable and taken as of $\epsilon_4 = 0$.

The TPSM wave function is expressed by means of the projection operator,

$$|\Psi_{IM}\rangle = \sum_{K\kappa} F^I_{\kappa,K} \hat{P}^I_{MK} |\Phi_\kappa\rangle, \tag{3}$$

in which the projected multi-QP states span the shell-model space. Where, $|\Phi_\kappa\rangle$ represents the set of multiquasiparticle states labeled by κ, and for even-even nuclei it includes the two- and four-QP states associated with the triaxially deformed QP vacuum $|0\rangle$,$\alpha^\dagger_{\nu_1}\alpha^\dagger_{\nu_2}|0\rangle$,$\alpha^\dagger_{\pi_1}\alpha^\dagger_{\pi_2}|0\rangle$,$\alpha^\dagger_{\nu_1}\alpha^\dagger_{\nu_2}\alpha^\dagger_{\pi_1}\alpha^\dagger_{\pi_2}|0\rangle$. The triaxially deformed single-particle states are generated by the Nilsson Hamiltonian. In the present TPSM calculation three major shells of $N = 4,5,6$ for neutrons and $N = 3,4,5$ for protons are considered, and the pairing correlations are included by a subsequent BCS calculation for the Nilsson states. $\hat{P}^I_{MK}$ in Eq. (3) is the three-dimensional angular-momentum-projection operator [5]. The rotational energies together with the wave functions, i.e., the coefficients $F^I_{\kappa,K}$, are obtained by solving the eigenvalue equation,

$$\sum_{K\kappa} F^I_{\kappa K}\big(\langle\Phi_{\kappa'}|H P^I_{K'K}|\Phi_\kappa\rangle - E^I\langle\Phi_{\kappa'}|P^I_{K'K}|\Phi_\kappa\rangle\big) = 0. \tag{4}$$

In the present approach, the sum of the liquid-drop and the shell-correction energies, $E_{LD} + E_{\rm corr}$ in Eq. (1), provides the energy of the deformed BCS vacuum state, relative to the spherical liquid-drop energy, and the rotational energy $E_{\rm rot}$ is calculated by Eq. (4), relative to the deformed QP vacuum. The total energy of the deformed nuclear system, $E^{\rm tot}$ in Eq. (1), is consequently defined in the laboratory frame, which is in function of spin and has also a good parity. The nuclear equilibrium deformation for each of the yrast or low-excited states can be obtained by minimizing their respective total energy with respect to the deformation parameters, ε_2 and γ. Once the PTES calculation is completed the minimization procedure can be performed simply through the finding of the local minimum in the total energy surface at a given spin.

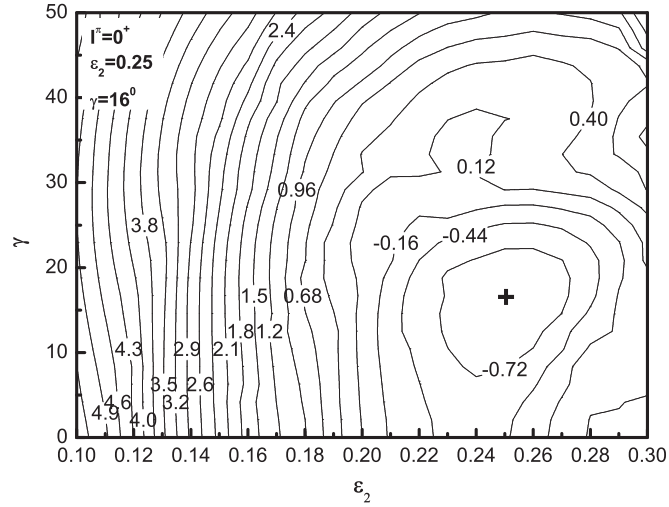

FIG. 1. Contour plot of total energy in units of MeV for the ground state of ^{172}W, the local minimum is marked by +.

III. RESULTS AND DISCUSSION

A. PTES for given angular momentum

All calculations of the projected total energy surfaces in the present work are carried out for a given angular momenta as well as a given parity; this allows us to obtain the nuclear states with good quantum numbers of spin and parity and, therefore, provides an opportunity to make a direct comparison between the theory and the experiment. The general features of the projected total energy surfaces for the ground state (GS) $I^\pi = 0^+$ are illustrated with the example of the ^{172}W in Fig. 1. In the present PTES calculations the range of the elongation deformation ε_2 is taken from 0.1–0.3, while the range of the triaxial deformation γ from 0°–50°, and the mesh points of 20 have been taken for both the ε_2 and γ deformations. Figure 1 shows that there exist a local minimum in the PTES for the GS of ^{172}W, which represents the equilibrium deformations of $(\varepsilon_2 = 0.252, \gamma = 16.4°)$. The results imply that the GS of the nucleus is well deformed, and it is particularly noteworthy to have a considerable axial asymmetry with $\gamma \sim 16°$. We will show that the triaxiality of a similar size appears in the yrast states of the $^{170-178}$W even-even isotopes, and the reason for that may be attributed to the beyond-mean-field effects.

B. PTES for the yrast states in the $^{170-178}$W isotopes

The PTES calculation for ^{172}W at the GS $I^\pi = 0^+$, demonstrated in the above subsection, has been extended to the yrast states of the $^{170-178}$W isotopes, up to spin 20. A local minimum is found in each of the 55 PTESs for spins of $I^\pi = 0^+,2^+,4^+,6^+,\ldots,20^+$ in the yrast bands of these five nuclei. These local minima allow to determine the equilibrium deformations (ε_2,γ) for each spin in the yrast states of the $^{170-178}$W isotopes, and the results are listed in Table I. Both the elongation and triaxial equilibrium deformations presents being almost unchanged from spin 0 up to 20 for each of $^{170-178}$W isotopes, characterizing well-deformed nuclei where the kinetic moment of inertial

TABLE I. Deformations of the yrast states of $^{170-178}$W isotopes determined by the energy minima in PTES for spins 0^+–20^+.

	I^π	0^+	2^+	4^+	6^+	8^+	10^+	12^+	14^+	16^+	18^+	20^+
^{170}W	ε_2	0.242	0.242	0.242	0.242	0.242	0.242	0.242	0.242	0.24	0.24	0.24
	γ	17.6°	17.6°	17.4°	17.2°	17.2°	17.2°	17.2°	17.2°	16.2°	16.2°	16°
^{172}W	ε_2	0.252	0.252	0.252	0.254	0.254	0.256	0.258	0.256	0.252	0.250	0.252
	γ	16.4°	16.4°	16.2°	16°	15.8°	16.2°	15.8°	15.2°	15.4°	15.6°	15.4°
^{174}W	ε_2	0.244	0.244	0.244	0.246	0.246	0.246	0.248	0.246	0.244	0.244	0.244
	γ	18.2°	18.2°	18.2°	18°	18°	18°	17.8°	18°	18.2°	18.4°	18.6°
^{176}W	ε_2	0.24	0.24	0.24	0.24	0.24	0.241	0.241	0.24	0.24	0.24	0.24
	γ	11.4°	11.4°	10.8°	10.4°	9.8°	9.6°	9.2°	9°	9°	9.4°	9.4°
^{178}W	ε_2	0.244	0.244	0.244	0.244	0.244	0.244	0.244	0.246	0.246	0.242	0.246
	γ	11.8°	11.8°	11.6°	11.4°	11°	10.6°	10.6°	10.4°	10.2°	11.4°	11.6°

does not considerably change with increasing spin. A slightly larger ε_2 deformation is found for the ground state of ^{172}W compared to other tungsten isotopes, and the fact is due to the shell effect, corresponding to the energy gap at $N = 98$ in the neutron single-particle diagram. The shell effect is well described within the mean-field approximation, which has been contained in the PTES approach. The validity of this argument may be verified by the TRS calculation, which results in a similar slight gain in the ε_2 deformation at the ground state of ^{172}W compared to other tungsten isotopes considered, see Table III. The calculated equilibrium γ deformations for the yrast states of $^{170-178}$W isotopes are considerably large, about $\gamma = 15°$ in average. It is striking because the pure mean-field approximation, for example, the TRS calculation, yields the equilibrium γ deformation of nearly zero for these light tungsten nuclei, see Table III. The appearance of the considerable large triaxiality may be attributed, therefore, to the beyond-mean-field effect associated with the rotational symmetry restoration of a triaxial-shaped system through the angular momentum projection.

The PTES for the each state is first calculated and then the minimization procedure with respect to the elongation and triaxial deformations is performed to obtain the energy of the state together with the equilibrium deformations, and in this way the yrast band is calculated self-consistently within the PTES approach. Figure 2 shows the calculated yrast bands for the $^{170-178}$W isotopes, the corresponding equilibrium deformations are given in Table I, compared with the experimental data [24,25]. It is seen that the calculated results are in good agreement with the experimental data.

C. Deformation changes in the $^{170-178}$W isotopes

The ε_2 deformation for each of the $^{170-178}$W isotopes presents almost unchange with increasing spin, characterizing the well-deformed rotor. A tiny change of ε_2 deformation has been found in the band interaction region, where the two-QP configuration comes into play. The elongation deformations for the five isotopes present very stable, the ε_2 values are about 0.24 for ^{170,174,176,178}Wand about 0.25 for ^{172}W, and this exceptional case has been explained as the shell effect in the previous section. In contrast to the stability of the elongation deformation the triaxial deformation presents a slight decreasing with increasing neutron number. The triaxial deformation of $\gamma \approx 17°$ is found for ^{170,172,174}W and a smaller value of $\gamma \approx 11°$ for ^{176,178}W. The γ deformation change of few degrees may be understood as the origin of the shell effects. The energy gap of $N = 98$ at around $\varepsilon_2 = 0.25$ in the neutron single-particle Nilsson diagram persists in a large range of the triaxial deformation, from $\gamma = 0°$–$30°$. The negative shell correction energy associated with the energy gap provides the basic condition for the formation of relatively large γ softness in ^{170,172,174}W, where the neutron Fermi level lies around the energy gap. On the other hand, a much less enhanced γ softness appears in ^{176,178}W as the neutron Fermi level lies well above the $N = 98$ energy gap. The addition of the quantal rotational energy could drive, therefore, the nuclear shape towards a larger γ deformation for ^{170,172,174}W than for ^{176,178}W.

The calculated equilibrium γ deformations of the ground states in $^{170-178}$W slightly decrease with the increasing neutron number. It is interesting to note that the energies of the observed γ-band heads in these nuclei present a slightly increasing with increasing neutron number. These two opposite variation tendencies with increasing neutron number might have their correlation, which is also implied in the TPSM calculations of the γ bands where a slightly decreasing γ deformation has

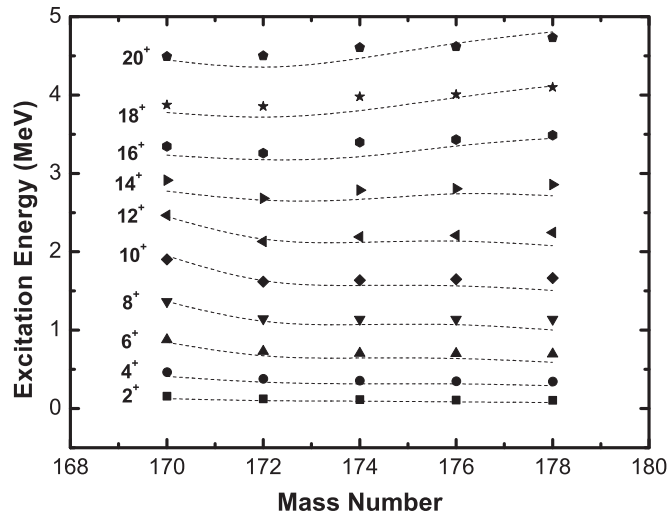

FIG. 2. Calculated yrast bands, the energy levels, for $^{170-178}$W isotopes compared with the experimental data.

TABLE II. Quadrupole deformations ε_2 and γ employed in the TPSM calculation for ground-state bands and their γ bands in $^{170-178}$W isotopes.

Nuclei	^{170}W	^{172}W	^{174}W	^{176}W	^{178}W
ε_2	0.242	0.252	0.244	0.240	0.244
γ	27.5°	25°	25°	24°	23°

to be employed to reproduce the experimental data when the neutron number increases, see Table II.

The transition quadrupole moments measured by using high-precision experimental techniques are one of best observables to provide a specific measurement of the quadrupole deformation. The transition quadrupole moments Q_t can be expressed as a function of quadrupole deformations (β_2, γ),

$$Q_t = \frac{6ZeA^{2/3}}{(15\pi)^{1/2}} r_0^2 \beta_2 \left[1 + \frac{2}{7}\left(\frac{5}{\pi}\right)^{1/2} \beta_2\right] \cos(30^\circ + \gamma). \quad (5)$$

The transition quadrupole moments Q_t of the yrast states in ^{170}W and ^{172}W were determined experimentally up to spin 20 by the lifetime measurements [26,27]. With the calculated equilibrium deformations (ε_2, γ) of the yrast states, as presented in Table I, the transition quadrupole moments of ^{170,172}W are calculated by using the equation above and taking $\beta_2 = \varepsilon_2/0.946$ and $r_0 = 1.280$fm. The calculated Q_t results are shown in Fig. 3 and compared with the experimental data of the lifetime measurements.

The agreement between theory and experiment is quite good except that the experimental data are rather smaller than theoretical values for the three yrast states of 10^+–14^+ in ^{170}W. The dropping behavior of Q_t observed at spin 10–14 remains to be understood, and, however, we should mention that the high accuracy of the lifetime measurement at the band interaction region was difficult to be ensured due to the complex γ-ray side feedings. Unfortunately, there are no more experimental Q_t data in the light tungsten isotopes to compare with the PTES calculations, and thus the theoretical results for other nuclei given in Table I need further experimental verifications.

D. Triaxiality and γ bands

The considerable triaxiality is found for $^{170-178}$W isotopes, the average value of the equilibrium triaxial deformation is $\gamma \sim 15^\circ$. The origin of the considerable large triaxiality is attributed to the beyond-mean-field effect as having addressed above. The observed low lying γ bands in the light tungsten isotopes may be regarded as the indirect evidence for the existence of the considerable triaxiality in these nuclei. In the TPSM calculations for the γ bands, the elongation deformations have been taken as the same as the equilibrium elongation deformations for the ground states $I^\pi = 0^+$, while the values of the γ deformation have been taken to reproduce the excitation energies of the γ bands, adopted deformation values seen in Table II. The present TPSM calculations well reproduce the experimental γ-band data as well as the ground-state bands, as shown in Fig. 4. To reproduce the γ bands a large γ deformation, $\sim 25^\circ$ has been taken, and the specific values for the light tungsten isotopes decrease slightly with increasing neutron number. The energy of the γ-band head is sensitive to the γ deformation. The small change of the γ deformation, about a few degrees, is crucial to reproduce the experimental data that the excitation energies of γ bands decrease with neutron number, from 0.937 MeV for ^{170}W, 0.930 MeV for ^{172}W, 0.977 MeV for ^{174}W, 1.042 MeV for ^{176}W, to 1.111 MeV for ^{178}W. The increase of γ value of $\sim 4^\circ$ leads to the lowering of 174 keV for the γ-band-head energy from ^{178}W to ^{170}W. It is a longstanding puzzle that many well-deformed nuclei through the nuclear chart for which the mean-field models predict the axial symmetry, $\gamma \sim 0^\circ$, the low-lying γ bands have been observed. The possible explanation for the phenomenon has been widely argued as the γ vibration around the prolate nuclear shape. The present PTES theory predicts a wide happening of the considerable triaxiality in the ground nuclear states, and, therefore, the understanding of the wide existence of the low-lying γ bands becomes more transparent, as the picture of the γ vibration around the axial symmetric shape is no longer a solid starting point for the modeling.

TABLE III. Deformations of the ground state of $^{170-178}$W isotopes determined by the energy minima in TRS at the rotational frequency of $\hbar\omega = 0.02\hbar\omega_0$.

Nuclei	^{170}W	^{172}W	^{174}W	^{176}W	^{178}W
ε_2	0.224	0.241	0.234	0.224	0.224
γ	−3°	2°	2°	−3°	−3°

E. Comparison between the PTES and TRS calculations

The total Routhian surface (TRS) approach has been intensively employed to study highly rotating nuclei, which is one typical nuclear model based on the mean-field approximation but without including of the beyond-mean-field effects. It is, therefore, instructive to make a comparison between the PTES and TRS calculations. The rotational frequency, as a classical term employed in the TRS approach has been a useful quantity to describe nuclear rotation. However, because of this semiclassical nature of the TRS method it is not possible to strictly describe the ground state, which has a good angular momentum of $I = 0$. It should be noticed that the quantum state with spin of $I = 0$ is a rotational one and does not match with the rotational frequency of zero. Usually, to describe the ground state of the nucleus, the TRS calculation may be, empirically, performed at a small rotational frequency, which is larger than zero and far below the band crossing frequency. As an example, the TRS for ^{172}W calculated at the rotational frequency of $\hbar\omega = 0.02\hbar\omega_0$, is shown in Fig. 5, which reports a local minimum at the deformations of $(\varepsilon_2 = 0.241, \gamma = 2^\circ)$. The calculated equilibrium elongation deformation by the TRS is similar to one calculated by the PTES, but much different equilibrium γ deformation is always generated from the TRS than the PTES. The value of $\gamma = 2^\circ$ from the TRS calculation indicates the axial symmetry for the ground state

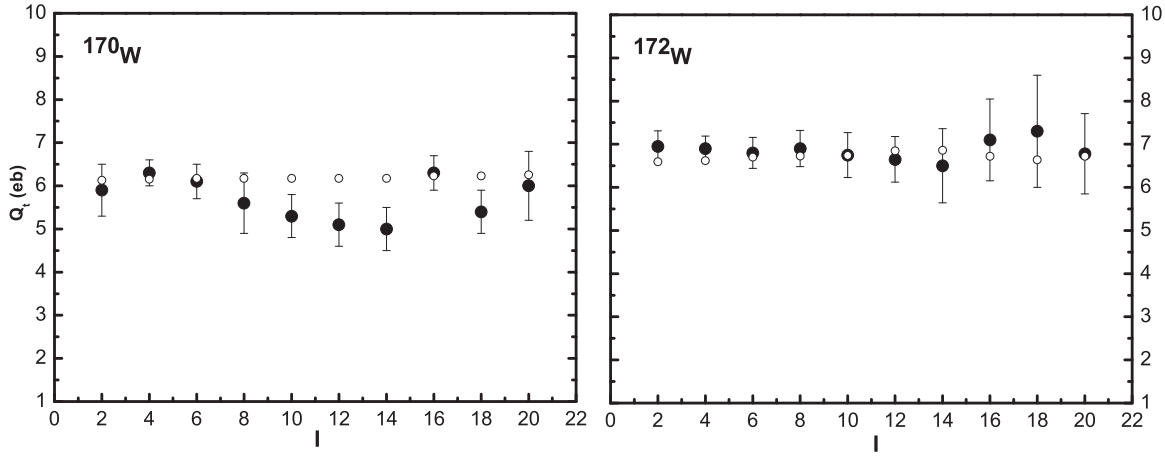

FIG. 3. Calculated transition quadrupole moments (open circle) in function of spin for the yrast bands of the ^{170,172}W, compared with the available experimental data (solid circle).

of ^{172}W, while the value of $\gamma = 16.4^\circ$ obtained from the PTES calculation implies the axial asymmetry nature for the GS of the same nucleus. Note that the present PTES and TRS calculations start with the same single-particle states and approximately same pairing interaction as well as the same model space truncation, and the major difference is the fact that the former contains the angular momentum projection but the latter does not. Therefore, we may safely conclude that the beyond-mean-field effect, associated with the angular momentum projection, is responsible for the origin of the significantly large triaxiality obtained from the PTES calculation.

Recently, the global calculation across the nuclear chart of axial symmetry breaking was carried out by using the macroscopic-microscopic finite-range liquid-drop model (FRLDM) [28,29]. Many nuclear ground states have been predicted to be triaxially shaped or γ soft by the FRLDM calculations, and some of which were previously predicted

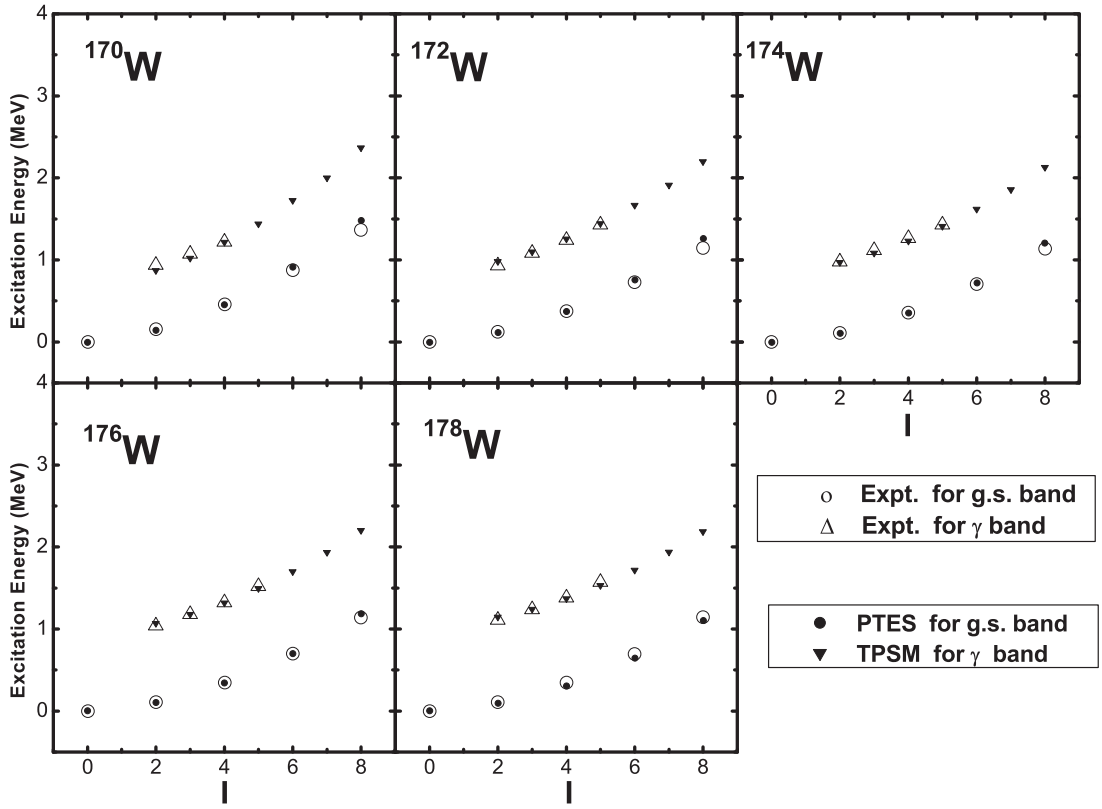

FIG. 4. Calculated ground-state bands and their γ bands (solid symbols), the energy versus spin, for $^{170-178}$W isotopes, and a comparison with the experimental data (open symbols).

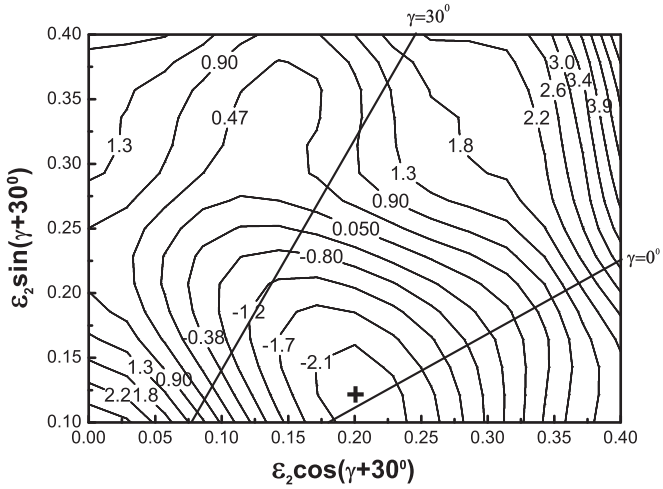

FIG. 5. Contour plot of total Routhian in units of MeV for ^{172}W, calculated at the rotational frequency $\hbar\omega = 0.02\hbar\omega_0$, the minimum is marked by +.

to be axial symmetric by the TRS calculations. The different results of the FRLDM than the TRS method come from their different parameterizations although the two methods belong to the same type of macroscopic-microscopic approach. For the light tungsten $^{170-178}$W isotopes, both the FRLDM and TRS calculations report an axial symmetry for the ground states. As shown in above sections, the present PTES calculation and TPSM calculation yields the axial asymmetry of ($\gamma \sim 15^\circ$) for ground-state bands and ($\gamma \sim 25^\circ$) for γ bands, respectively. The larger γ deformation predicted with the PTES and TPSM calculations than the FRLDM calculations confirms again the beyond-mean-field effects on the nuclear triaxiality.

The PTES/TPSM approach treats the nuclear rotation quantum mechanically and allows three-dimensional rotation through the angular momentum projection. In contrast, the TRS/CSM method (not tilted cranking) treats only the semiclassical rotation and requires the system to rotate around the shortest principle axis with a rotational frequency. The beyond-mean-field effect incorporated in the PTES/TPSM approach is the quantal effect, which favors the triaxial rotation. Recently, the first study of the full projected mean field was performed for the even-even *sd* nuclei by using the USDB Hamiltonian. The calculated results show that the intrinsic shapes of the variation-after-projection (VAP) wave functions with angular momentum projection are always triaxial while the usual HFB methods provide axial shapes [30]. In addition, early other calculations of triaxial deformation and its effect on the low-energy nuclear structure phenomena performed by Bender *et al.* [31,32] using beyond-mean-field calculations based on the nonrelativistic Skyrme energy density functionals, by Rodriguez *et al.* [33,34] and Delaroche *et al.* [35] using beyond-mean-field calculations based on the Gogny DIS interaction, and by Yao *et al.* [36], by Niksic *et al.* [37,38] using relativistic energy density functionals, come to a similar conclusion that beyond-mean-field effects play an important role in nuclear triaxiality.

F. Decomposition of energy surface

To study the beyond-mean-field effect associated with the angular momentum projection in further details the component energy surfaces have been calculated as a decomposition of the PTES. The calculated component energy surfaces for ^{172}W are shown in Fig. 6(a) for the $E_{LD} + E_{\rm shell}$ and Fig. 6(b) for the $E_{\rm rot}$. The liquid-drop model plus shell energy surface presents a local minimum at the axial symmetry with the $\varepsilon_2 \sim 0.24$, and the flatness of the surface around the minimum indicates a modest γ softness towards the γ deformation direction. The rotational energy surface for the spin $I = 0$, shown in Fig. 6(b), presents the striking feature to drive the ε_2 deformation towards a larger elongation and the γ deformation from both 0° (prolate) and 60° (oblate) axial symmetric shapes towards about 25°. It is seen that the projected rotational energy at $\varepsilon_2 = 0.24$ can generate a significant enough driving force in the γ direction to provide a lowering of the total energy in the laboratory frame by about 600 KeV from the axial symmetry to the triaxiality of $\gamma \sim 16^\circ$.

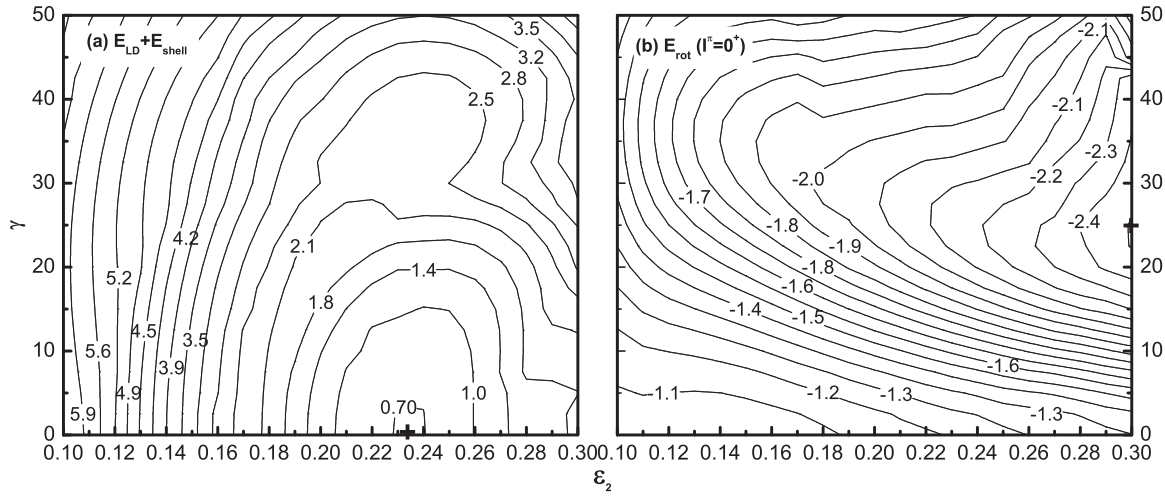

FIG. 6. Component energy surfaces of the total energy for the ground state of $I^\pi = 0^+$ in ^{172}W: (a) $E_{LD} + E_{\rm shell}$ and (b) $E_{\rm rot}$. The energy is in units of MeV.

The $E_{LD} + E_{\text{shell}}$ surface shown in Fig. 6(a) applies also to the present TRS calculation so that the TRS shown in Fig. 5 can be regarded as the result by adding the rotational energy given by CSM to the liquid drop plus shell energy. The axial symmetric shape described by the local minimum in the $E_{LD} + E_{\text{shell}}$ surface remains unchange in the TRS, implying that the γ-deformation driving effect promised from adding the classical rotational energy defined in the TRS approach is not sufficient to cause the formation of a local triaxial minimum in the TRS. In contrast, the quantal rotational energy surface such as one shown in Fig. 6(b) can provide the strong γ-deformation driving in the formation of the axial asymmetry shapes of the yrast states in ^{172}W.

Although a direct comparison between the quantal and classical rotational energies is not possible but it can be seen that at $\varepsilon_2 = 0.24$ the energy lowering from $\gamma = 0^\circ$ towards 15° is about 0.1 MeV for the classical rotation in the TRS at $\hbar\omega = 0.02\hbar\omega_0$, estimated by reading data from Fig. 5 and Fig. 6(a), and, however, it is about 0.6 MeV for the quantum rotation in the PTES at $I^\pi = 0^+$, estimated from Fig. 6(b). These results indicate that in the nuclear energy surface calculations the inclusion of the angular momentum projection, as the beyond-mean-field effects, is crucial in the study of nuclear symmetry and symmetry break. We would like to emphasize that the quantal nuclear state at an angular momentum $I = 0$ is a certain rotational state, which has the same essential nature as the one at $I > 0$, and the rotational energy surfaces at $I = 0$ and $I > 0$ will have a similar structure. However, the cranking nuclear state at the frequency $\hbar\omega = 0$ is not a rotational state, and the nuclear rotation is described at the frequency $\hbar\omega > 0$ in the CSM picture. Consequently, there is the fatal problem in the CSM to describe strictly the nuclear ground state that has a quantum number of $I = 0$.

IV. CONCLUSIONS

The restoration of the rotational symmetry plays a crucial role in the nuclear mean-field modeling of the system with the axial asymmetric shape. This has been realized in the PTES approach through the procedure of the variation after the angular momentum projection. The angular momentum projection, known as the beyond-mean-field treatment, allows us to generate the total energy surface for a given spin as well as parity. The projected total energy surfaces calculated for the yrast states of $^{170-178}$W even-even isotopes present the local triaxial minima corresponding to the elongation equilibrium deformation of $\varepsilon_2 \sim 0.24$ and the triaxial deformation of $\gamma = 17^\circ$–11°. In contrast, the TRS calculations, as the typical mean-field approximation, yield the axial symmetric equilibrium shapes with the quadrupole deformations of ($\varepsilon_2 \sim 0.23, \gamma \sim 2^\circ$) for the GS of the same nuclei. The experimental data of the yrast states of $^{170-178}$W have been well reproduced by the present PTES calculation. The calculated transition quadrupole moments (Q_t) in function of spin are in nice agreement with the available lifetime measurement data in ^{170,172}W. By using the equilibrium elongation deformation determined by the PTES calculation and the γ deformation of $\gamma \sim 25^\circ$, the TPSM calculations well reproduce the experimental excited γ bands of $^{170-178}$W. The beyond-mean-field effects incorporated in the PTES approach through the angular momentum projection are responsible for the origin of the significant triaxiality predicted by the PTES calculations for the previously known axial symmetric nuclei such as the light tungsten isotopes.

ACKNOWLEDGMENTS

The work is supported by National Nature Science Foundation of China under Grants No. 11301508, No. 11047171, No. 11175258, No. 11575290, No. 11205246, and by the Knowledge Innovation Project of the Chinese Academy of Sciences under Grant No. KJCX2-SW-N02, the Key Project of Science and Technology Research of Education Ministry of China under Grant No. 209053, National Key Research and Development Project No. 2016YFA0400502, and joint fund of the National Natural Science Foundation of China and China Institute of Engineering Physics (Grant No. U1430114).

[1] A. Bohr and B. R. Mottelson, *Nuclear Structure* (Benjamin, New York, 1969 and 1975), Vols. I and II.
[2] P. Ring and P. Schuck, *The Nuclear Many-Body Problem* (Springer, Berlin, 1980).
[3] J. L. Wood, K. Heycle, W. Nazarewicz, M. Huyse, and P. Van Doppen, Phys. Rep. **215**, 101 (1992).
[4] Tu Ya, Y. S. Chen, Z. C. Gao, S. Y. Yu, and L. Liu, Sci. China Phys. Mesh. Astron. **57**, 2054 (2014).
[5] Z. C. Gao, Y. S. Chen, and Y. Sun, Phys. Lett. B **634**, 195 (2006).
[6] K. Nomura, T. Otsuka, R. Rodríguez-Guzmán, L. M. Robledo, and P. Sarriguren, Phys. Rev. C **84**, 054316 (2011).
[7] K. Nomura, T. Otsuka, R. Rodríguez-Guzmán, L. M. Robledo, P. Sarriguren, P. H. Regan, P. D. Stevenson, and Zs. Podolyák, Phys. Rev. C **83**, 054303 (2011).
[8] R. Bengtsson and T. Bengtsson, J. Dudek, G. Leander, W. Nazarewicz, and J. Y. Zhang, Phys. Lett. B **183**, 1 (1987).
[9] W. Nazarewicz, M. A. Riley, and J. D. Garrett, Nucl. Phys. A **512**, 61 (1990).
[10] Z. S. Podolyák and P. H. Regan *et al.*, Phys. Lett. B **491**, 225 (2000).
[11] M. Camaano and P. M. Walker *et al.*, Eur. Phy. J. A **23**, 201 (2005).
[12] P. M. Walker and T. R. Xu, Phys. Lett. B **635**, 286 (2006).
[13] W. D. Myers and W. Swiatecki, Ark. Fys. **36**, 343 (1967).
[14] V. M. Strutinsky, Nucl. Phys. A **95**, 420 (1967).
[15] V. M. Strutinsky, Nucl. Phys. A **122**, 1 (1968).
[16] W. Nazarewicz, J. Dudek, R. Bengtsson, T. Bengtsson, and I. Ragnarsson, Nucl. Phys. A **435**, 397 (1985).
[17] Tu Ya, Y. S. Chen, S. Y. Yu, C. W. Shen, Z. C. Gao, Y. J. Chen, and L. Liu, Nucl. Phys. A **848**, 260 (2010).
[18] W. Satula, R. Wyss, and P. Magierski, Nucl. Phys. A **578**, 45 (1994).
[19] F. R. Xu, W. Satula, and R. Wyss, Nucl. Phys. A **669**, 119 (2000).
[20] C. F. Jiao, J. C. Pei, and F. R. Xu, Phys. Rev. C **90**, 054314 (2014).

[21] C. F. Jiao, Yue Shi, H. L. Liu, F. R. Xu, and P. M. Walker, Phys. Rev. C **91**, 034309 (2015).
[22] T. Bengtsson and I. Ragnarsson, Nucl. Phys. A **436**, 14 (1985).
[23] K. Hara and Y. Sun, Int. J. Mod. Phys. E **04**, 637 (1995).
[24] J. Espino and J. D. Garrett *et al.*, Nucl. Phys. A **567**, 377 (1994).
[25] T. Kibédi and G. D. Dracoulis, A. P. Byrne, and P. M. Davidson, Nucl. Phys. A **688**, 669 (2001).
[26] F. K. Mcgowan, N. R. Johnson, I. Y. Lee, C. Baktash, J. W. McConnell, M. N. Rao, M. Oshima, J. C. Wells, A. Larabee, L. L. Riedinger, R. Bengtsson, and Z. Xing, Nucl. Phys. A **530**, 490 (1991).
[27] F. K. Mcgowan and N. R. Johnson, M. N. Rao, C. Baktash, I. Y. Lee, J. C. Wells, M. Kortelahti, and V. P. Janzen, Nucl. Phys. A **580**, 335 (1994).
[28] P. Möller and R. Bengtsson, B. G. Carlsson, P. Olivius, and T. Ichikawa, Phys. Rev. Lett. **97**, 162502 (2006).
[29] P. Möller, A. J. Sierk, R. Bengtsson, H. Sagawa, and T. Ichikawa, At. Data Nucl. Data Tables **98**, 149 (2012).
[30] Z. C. Gao, Mihai Horoi, and Y. S. Chen, Phys. Rev. C **92**, 064310 (2015).
[31] M. Bender and P. H. Heenen, Phys. Rev. C **78**, 024309 (2008).
[32] B. Bally, B. Avez, M. Bender, and P. H. Heenen, Phys. Rev. Lett. **113**, 162501 (2014).
[33] T. R. Rodríguez and J. L. Egido, Phys. Rev. C **81**, 064323 (2010).
[34] T. R. Rodríguez, Phys. Rev. C **90**, 034306 (2014).
[35] J.-P. Delaroche, M. Girod, J. Libert, H. Goutte, S. Hilaire, S. Péru, N. Pillet, and G. F. Bertsch, Phys. Rev. C **81**, 014303 (2010).
[36] J. M. Yao, J. Meng, P. Ring, and D. Vretenar, Phys. Rev. C **81**, 044311 (2010).
[37] K. Nomura, N. Shimizu, D. Vretenar, T. Nikšić, and T. Otsuka, Phys. Rev. Lett. **108**, 132501 (2012).
[38] T. Nikšić, P. Marević, and D. Vretenar, Phys. Rev. C **89**, 044325 (2014).